IOP PUBLISHING JOURNAL OF PHYSICS D: APPLIED PHYSICS

J. Phys. D: Appl. Phys. **41** (2008) 224006 (9pp) doi:10.1088/0022-3727/41/22/224006

Holographic data storage in photorefractive bismuth tellurite

W Horn[1], I Földvari[2] and C Denz[1]

[1] Institut für Angewandte Physik, Westfälische Wilhelms-Universität, Münster, Germany
[2] Research Institute for Solid State Physics and Optics, Hungarian Academy of Sciences, Budapest, Hungary

E-mail: w.horn@uni-muenster.de

Received 19 March 2008, in final form 16 July 2008
Published 24 October 2008
Online at stacks.iop.org/JPhysD/41/224006

Abstract
Bismuth tellurite is a photorefractive material for holographic data storage offering unique fixing capabilities. Important material and electro-optic properties obtained by four-wave-mixing and data storage experiments are reviewed and recent results concerning the applicability of bismuth tellurite for holographic data storage, including dynamic range, multiplexing capabilities and bit-error evaluations, are presented. Furthermore, it is demonstrated how the latest progress in growing Bi_2TeO_5 made this crystal a candidate for durable holographic recording media.

1. Introduction

Data storage based on volume holography has been the subject of comprehensive research during the last decade. Besides high data density, volume phase holography offers fast access speed [1], high data throughput and enables associative searching procedures [2]. These features can be achieved by multiplexing large stacks of digital data pages in one spatial storage location. Up to now, the main shortcomings of holographic data storage involving photorefractive rewriteable media are slow recording speeds, volatility of data and insufficient long-term stability. These deficiencies are generally related to electro-optical processes in inorganic solid state materials. Different materials for volume holographic data storage have been investigated in the past, including inorganic photorefractive crystals, photopolymers, photo-addressable polymers, photorefractive polymers and thermoplastics [3]. Unfortunately, none of those materials is able to offer all the characteristics required. The most important attributes include absorption, scattering, sensitivity, dynamic range, optical quality, read-out fidelity, long-term stability, write–erase capability, interchangeability, thickness and production costs. Since all inorganic crystals enabling read–write access suffer from volatile index modulation, different fixing techniques for long-term storage have been proposed. Among them are thermal fixing [4], two-colour writing [5] and fixing by external electric fields [6]. All these techniques require additional system complexity and are less suited for practical implementation. Bismuth tellurite for holographic data storage applications has been investigated extensively due to its unique fixing capabilities. Recorded holograms do not require any further treatment and provide partial non-volatile read out [7].

In section 2 of this review the development of the material itself is reported and a brief explanation of chemical compounds, composition and growth is given. In section 3, the characterization of the storage material is explained and the results of elementary laser induced gratings with different dopants under various crystal orientations are illustrated. Section 4 deals with high capacity page-wise storage of analog and digital data used to examine the applicability of Bi_2TeO_5 crystals for holographic storage systems.

2. Properties of bismuth tellurite

Bismuth tellurite crystallizes in an orthorhombic structure (*mm*2) and the crystal is optically biaxial without centre of symmetry. The crystal structure can be described as a $2 \times 3 \times 1$ multiplication of a CaF_2-type cell [8]. The required cation charge is 4+ in this lattice and the missing charge of the Bi^{3+} ions is compensated by a large number (17%) of empty oxygen positions. Three different Bi-sites were identified in the Bi_2TeO_5 structure surrounded by 7 and 8 oxygens, respectively. Tellurium keeps the unique, strongly asymmetric, covalent local structure of the tellurium–oxygen compounds, forming a trigonal pyramidal arrangement with 3 oxygens and tellurium

at the points of the pyramid. Two more oxygens are present around the Te with ionic distance. The material follows the peculiar oxidation behaviour of the tellurium oxide based binary oxides, which may form both tellurites (with Te^{4+} nominal charge) and tellurates (with Te^{6+}) [9].

Single crystals of Bi_2TeO_5 can be grown from the melt. The difficulties in the crystal growth are related to the cation and oxygen stoichiometry. At the melting point of Bi_2TeO_5, the evaporation of the TeO_2 component is significant, and there is only a narrow solid phase homogeneity range for single crystals where the Bi_2TeO_5 crystal structure exists. The melt composition for growing single crystals with acceptable quality is limited to 50–52.5 mole % TeO_2 [10]. In the Te-rich part of this range of the Bi_2TeO_5 only intrinsic absorption is observed, obeying the Urbach rule [11]. In this type of crystal the absorption of the 532 nm Nd : YAG line is due to the tail of the intrinsic absorption edge. The reproducible growth technique for this crystal composition has been established [10]. On the other hand, the Bi-rich crystal exhibits additional absorption bands in the transparent spectral region which was typical of the early crystals [12]. The origin of this coloration and its thermal instability was pointed out in [13]. A similarity to the sillenites was suggested, where the coloration was attributed to anti-site Bi-ions [13].

The Bi_2TeO_5 crystal is stable at room temperature, and the oxidation to tellurate (Bi_2TeO_6) begins at about 550 °C. However, this process is kinetically blocked in single crystals [14]. The tellurate produced then decomposes again at higher temperatures (about 700 °C), losing oxygen and recovering the tellurite composition. Consequently, the tellurite composition (Bi_2TeO_5) crystallizes from the melt but the pulled crystal goes through a temperature region in which partial oxidation to tellurate may happen. The oxygen equilibrium can be characterized by the intensity of the 762 cm^{-1} Raman line in a specific orientation and light propagation configuration [15]. Accordingly, the oxygen excess in the Czochralski grown crystals is not significant. The starting material for crystal growth was prepared by a two step solid phase reaction of TeO_2 and Bi_2O_3. The diameter controlled Czochralski technique was applied for crystal growth [16]. Platinum crucible and open air furnace (air ambient) were satisfactory for growth. The crystals were pulled along the ⟨0 0 1⟩ crystallographic axis, with a diameter of 25 mm, at pulling rates of 0.8–1 mm h^{-1} and rotation speed of 12–15 rpm. The strong optical anisotropy of the Bi_2TeO_5 crystals requires precise orientation of the samples that was performed by the x-ray diffraction technique. There is a cleavage plane (1 0 0), along which mirror flat surfaces can be obtained by simple cleaving. For other orientations the crystals were cut by precision cutting. Optical, microscopic and spectroscopic methods were used for general characterization of the crystals [11, 17].

Some of the important physical parameters for the photorefractive process are collected in table 1. The thermal and electric field dependence of the dark conductivity suggests an ionic hopping mechanism [18]. Charge carriers are the O^{2-} ions, and their migration is based on the large number of open oxygen positions. The charge carriers in photoconductivity are likely electrons [19].

Table 1. Crystallographic data and selected physical properties of Bi_2TeO_5 single crystals.

Property	Value
Crystal structure [8]	Orthorhombic, *Abm*2
Unit cell parameters (nm) [8]	$a = 1.16$, $b = 1.646$, $c = 0.552$
Density (g cm^{-3}) [16]	7.91
Melting point (°C) [16]	900–920
Optical transparency range (nm) [16]	400–7000
Refractive indices (at 632.8 nm) [20]	$n_a = 2.3203$, $n_b = 2.3678$, $n_c = 2.4022$
Nonlinear abs. coeff. (cm GW^{-1}, 532 nm) [21]	3.0–4.7

3. Volume holographic gratings

The principle of high capacity, volume phase holography is to overlap two coherent fields where one of the beams is the so-called signal beam that carries the information to be stored. The reference beam is used to establish a fixed phase relation to the signal field. Information on the signal beam is commonly imprinted by LCD, LCOS or MEMS arrays with a high resolution and digital access. Recording geometries for holographic data storage favour a precise Bragg selectivity to achieve high spectral resolution by multiplexing a large number of holograms in the same volume and thereby supplying a very high storage density throughout the recording media. Different multiplexing schemes have been proposed including angular- [22], wavelength- [23], shift- [24], peristrophic- [25] and phase-code-multiplexing [26].

The index change in materials such as $LiNbO_3$ and Bi_2TeO_5 is evoked by the photorefractive effect [27]. Photorefractive materials are inorganic electro-optic and photoconductive materials that exhibit nonlinear dynamics with laser power in the microwatt range. Charge carriers from impurities inside the bandgap, usually dopants in the crystal lattice in different valence states, can be excited into the conduction band where they migrate due to different charge transport processes such as diffusion, drift or the photovoltaic effect. After migration, charge carriers recombine from the conduction band into the impurity traps and an electric field builds up due to the charge carrier distribution. Subsequent electric fields give rise to a phase-shifted refractive index modulation via the electro-optic effect [28].

To measure basic photorefractive parameters, the output of a laser is split up by a polarizing beam splitter. Input polarizations and modulation depth are adjusted by waveplates. The diffracted signal is detected by a photodiode. Two writing conditions are commonly used where the beam crossing angle was 90° outside the sample (figure 1). The beam polarization is chosen either perpendicular or parallel to the grating vector.

3.1. Previous experiments

The first observation of the photorefractive effect in Bi_2TeO_5 crystal was published in 1991 [29]. In these experiments,

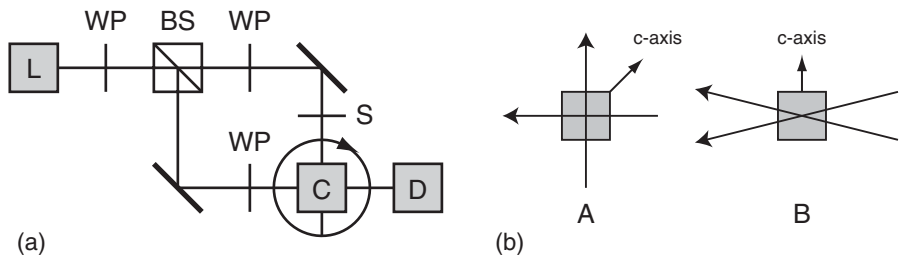

Figure 1. Setup for measuring diffraction efficiencies (*a*) in the two main crystal geometries (*b*). C : photorefractive crystal; D : photodiode; S : shutter; HW : half-wave-plate; BS : beamsplitter.

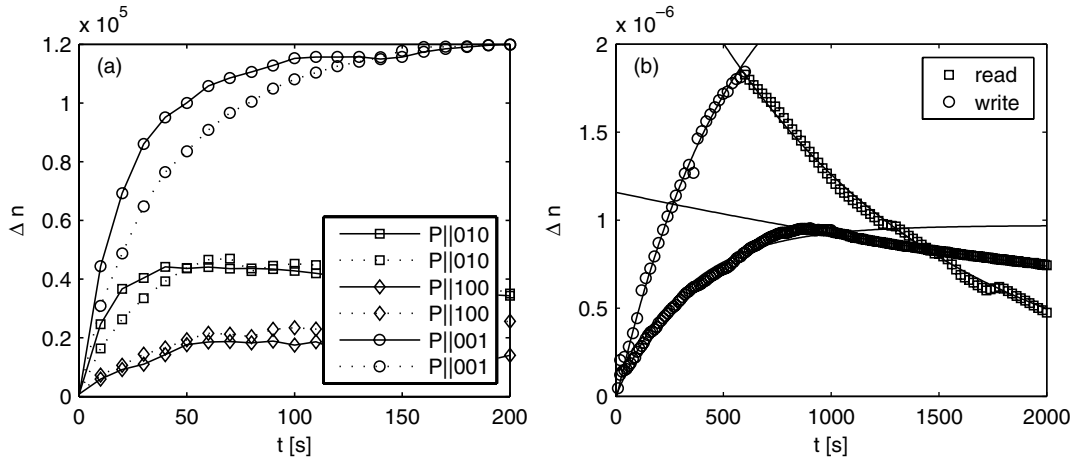

Figure 2. Typical refractive index change of undoped crystals in different writing geometries (*a*). Lines are a guide to the eyes. Read/write cycle (*b*); solid lines are monoexponential fitting curves.

the 514 nm output of a cw Ar–ion laser was used for writing diffractive gratings. Detailed investigations of the photorefractive effect with four-wave-mixing revealed an interesting material response. Besides the two fast components of the dark decay of the photorefractive signal (about 10 s and few minutes, respectively), a long living grating component was discovered that lasted for years in the dark and was difficult to erase by homogeneous light exposure [30]. This effect was named *self-fixing* since it resembled the stability of holograms fixed by different after-write techniques in $LiNbO_3$ crystal. The best explanation of self-fixing is related to the large number of open oxygen positions in Bi_2TeO_5. Accordingly, the oxygen ions migrate in the space charge field generated by the interference light pattern and subsequent electron replacement. The consequence is a reduced or compensated space charge field and an electrically neutral density modulation of the oxygen ions which leads to a local refractive index change.

The major problem in the photorefractive performance of Bi_2TeO_5 was the low saturation diffraction efficiency (2×10^{-3}) [31] which has been slightly enhanced (10^{-2}) by improving the crystal quality and the optical system [10]. Major improvements in the photorefractive performance of Bi_2TeO_5 have been achieved by using solid-state cw Nd : YAG lasers (532 nm) for writing diffraction gratings [32]. In the optimum grating vector configuration 44% saturation diffraction efficiency has been achieved. It was interesting that the maximum efficiency was experienced in a grating vector direction where the pure electro-optic effect was not expected from the crystal symmetry.

3.2. Continuous illumination

Two major orientations of the crystals have been investigated in detail as they are interesting for storage applications. In the first configuration, the two beams are incident on different perpendicular crystal faces and the grating vector is oriented 45° to the [1 0 0] crystallographic direction ($G \parallel 45°$ [1 0 0], $P \parallel$ [0 0 1]). In the second configuration, the beams are incident on one of the same basic planes with the grating vector parallel to the crystal surface ($G \parallel$ [0 0 1], $P \parallel$ [0 1 0]). Tests were usually carried out at room temperature and the samples are thermally treated for 8 h at 300 °C to remove the remaining holograms between successive measurements. According to coupled wave theory [33], the refractive index change is calculated by $\eta = \sin^2[(\Delta n \pi d)/(\lambda \cos \Theta)]$ and the holographic sensitivity $S = [(\sqrt{\eta})/(Id)]$, where d, Θ, λ and I are the crystal thickness, Bragg angle, writing wavelength and total recording intensity, respectively.

Figure 2(*a*) illustrates common grating build-up and erasure dynamics of the refractive index change of an undoped crystal under continuous illumination. The write and erasure intervals are 500 s, respectively, and the power density is 6 W cm^{-2}. The writing curve shows a multi-component development and time constants for the writing and reading process of Bi_2TeO_5 are different. A maximum refractive index change of more than 10^{-5} was obtained from undoped samples. The most common behaviour observed is illustrated in figure 2. The highest refractive index change could be obtained for a polarization in the $P \parallel$ [0 0 1] direction. In this configuration,

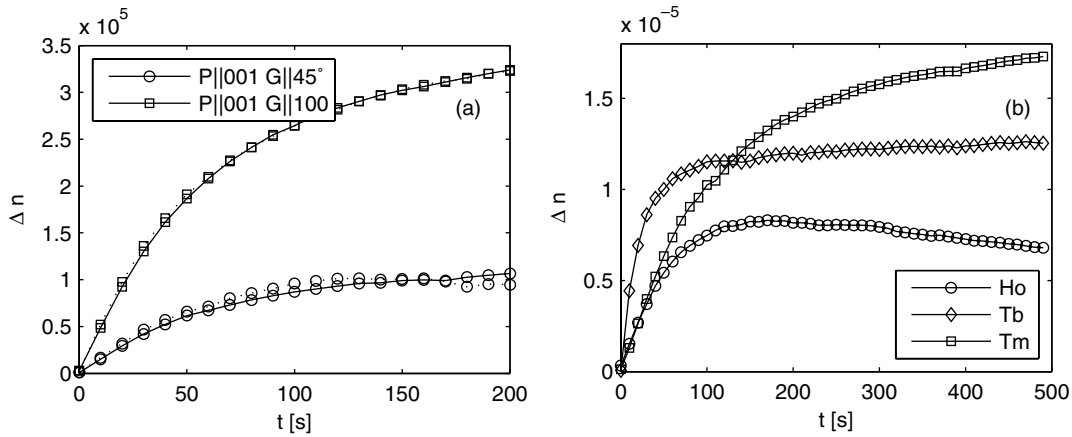

Figure 3. Refractive index change dependence of the crystal geometry in a holmium doped crystal (*a*). Typical refractive index change for dopants Ho, Tb and Tm (*b*). Lines are a guide to the eye.

the [1 0 0] crystallographic direction is parallel to the grating vector G. In other directions, only a 30% fraction of the maximum index modulation is observable.

The competitive saturation diffraction efficiency has opened new possibilities of employing the self-fixed photorefractive signal component in holographic recording. The durability of the holograms was also investigated in the dark (sequential reading) and during permanent read-out [7, 34, 35]. The hologram was readable in Bi_2TeO_5 after 8 h permanent reading while under the same writing geometry and power density it disappeared in the reference $LiNbO_3$: Fe crystal within 10 min [7, 34].

3.3. Dopants

To improve the dynamic range and reduce scattering for storage purposes, different dopants have been introduced into the crystal lattice. The ability of Bi_2TeO_5 crystals to adopt dopants shows a wide variety depending on the charge and bond covalence of the doping ions. Rare earth ions occupy three slightly different Bi^{3+} sites [36] with segregation coefficients close to unity [17]. In practice, this implies a homogeneous and high rate of dopant incorporation. Chromium substitutes for Te sites in the form of Cr^{6+} (chromate anion) [37]. The Cr incorporation includes an excess oxygen, filling a structural oxygen vacancy. Some other dopants such as iron exhibit a very low segregation rate, and the dopant is often in the form of aggregates or precipitates, reducing the optical quality of the crystal. This limits the present investigations for selected dopants. The dopant concentration is determined by the atomic absorption spectroscopic technique [38]. Spectroscopic properties, which are important for investigating the photorefractive effect in doped crystals, were determined for Cr [37], Er [39, 40], Tm [41], Yb [42], Ho [43] and Tb (unpublished).

Introducing dopants changes the photorefractive response significantly. In general, three different types of build-up kinetics can be observed: a single monotonic increase with a flat saturation, a build-up followed by a weak decay and a fast build-up followed by a slow increase in the diffraction efficiency. Undoped and Ho-doped crystals exhibit a high holographic sensitivity. This is due to the fact that Ho-doped crystals have sharp absorption lines at the excitation wavelength of the laser. However, holmium crystals suppress the crystal's ability to record a hologram in the 90° geometry. In Tb-doped crystals, the diffracted power was low because of its strong absorption. Terbium usually acts only as a charge trap, not as a source. Oxidized crystals were more than an order of magnitude more absorbing at the excitation wavelength and oxidized crystals are the most sensitive to the 532 nm wavelength. In Tm-doped crystal grating development is unstable and degrades very fast which is disadvantageous for long-term data storage. Common grating build-up kinetics are illustrated in figure 3.

The different doped Bi_2TeO_5 crystals exhibited a wide range of photorefractive responses. The saturation diffraction efficiency, saturation refractive index change and sensitivity obtained from different sample types and orientations are summarized in table 2.

3.4. Pulsed illumination

Measuring diffraction efficiencies by diffracted laser pulses from the holographic grating bears many problems and therefore a commonly used method is to employ a Bragg-matched cw laser at a different wavelength. Using this method, it is possible to collect data in real time with a high temporal resolution during the illumination of the pulses. The probe laser has to be adjusted to match the Bragg condition. A precise matching is necessary, since in the setup the angular half-widths are very small and a deviation from the Bragg angle would cause a large drop in diffraction efficiency. The diffracted He–Ne read out beam is separated from the reflected and scattered pump light in front of the detector. The setup has to be adjusted to obtain an optimal temporal and spatial overlap of the two beams.

When Bi_2TeO_5 is illuminated by intense strong laser pulses, light induced absorption changes are observed. The changes can be monitored with the weak probe beam and are much higher than those predicted and observed in lithium niobate crystals. The transient absorption changes are present when several traps with a different absorption cross-section

Table 2. Saturation diffraction efficiency, saturation refractive index change and photorefractive sensitivity of Bi_2TeO_5 crystals for different orientations and beam polarization configurations. E and G indicate the direction of the polarization and the grating vector.

Crystal	Orientation	η (10^{-3})	Δn (10^{-5})	S (10^{-3} cm J^{-1})
Bi_2TeO_5	$E \parallel [0\,0\,1]$ $G \parallel 45°[1\,0\,0]$	1.8	1.6	14.9
Bi_2TeO_5	$E \parallel [0\,0\,1]$ $G \parallel [0\,1\,0]$	10.2	3.9	12.7
Bi_2TeO_5	$E \parallel [0\,0\,1]$ $G \parallel [0\,0\,1]$	1.2	1.3	5.7
Bi_2TeO_5	$E \parallel [0\,1\,0]$ $G \parallel [0\,1\,0]$	1.2	1.3	1.6
Bi_2TeO_5 (oxidized)	$E \parallel [0\,0\,1]$ $G \parallel 45°[1\,0\,0]$	1.5	1.5	17.3
Bi_2TeO_5 : Ho	$E \parallel [0\,0\,1]$ $G \parallel 45°[1\,0\,0]$	1.1	1.3	2.0
Bi_2TeO_5 : Ho	$E \parallel [0\,0\,1]$ $G \parallel [0\,1\,0]$	9.4	3.7	11.1
Bi_2TeO_5 : Tb	$E \parallel [0\,0\,1]$ $G \parallel 45°[1\,0\,0]$	1.3	1.4	9.6
Bi_2TeO_5 : Tm	$E \parallel [0\,0\,1]$ $G \parallel [101]$	7.9	3.4	9.3

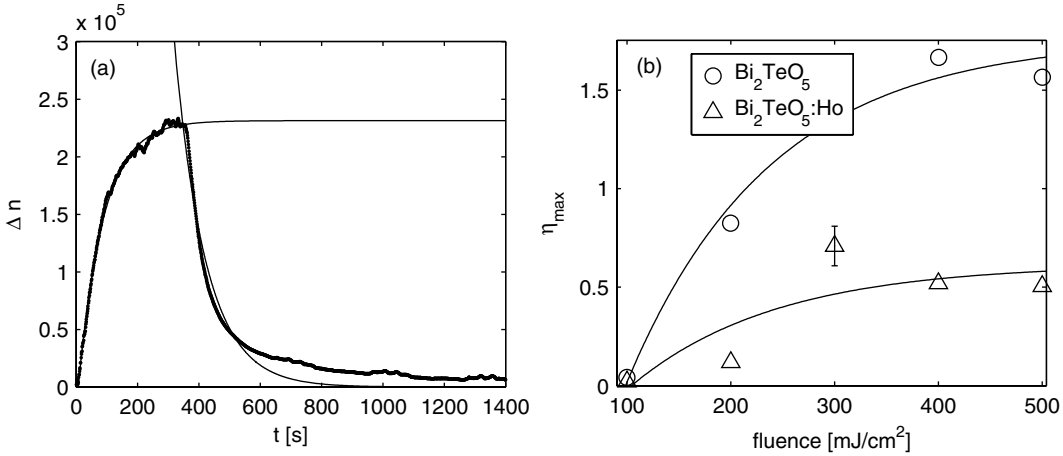

Figure 4. Typical behaviour of refractive index change (a). Dependence of the fluence and diffraction efficiency for undoped and holmium doped crystals (b). Solid lines are monoexponentially fitted curves. The repetition rate was 10 Hz at the 532 nm wavelength in 90° geometry.

participate in the charge transport [44]. In contrast to lithium niobate, time constants of transient absorption changes are in the range of several seconds and depend on the pump intensity. An offset from the original base absorption was noticeable, as the original state could only be obtained by long time thermal heating.

The temporal evolution of the photorefractive signal has been investigated by short pulse laser write experiments with pulse lengths at pico- and nanosecond timescales [45, 46]. After the strong diffraction peak due to temporary polarization by the electric field by overlapping 18 ps laser pulses, a diffraction component with decay of nanoseconds has been observed. The actual decay depends on the grating distance and this signal component was attributed to generation, spatial displacement and decay of free carriers [45]. It has been shown that with the used laser fluence, the two-photon absorption in the excitation process was significant [21].

A typical writing sequence during the storage process for a grating consists of 100 ns pulses with a maximum of 15 mJ cm^{-2} at 10 Hz repetition rate. This adds up to a total writing time of about 0.25 s and is usually sufficient for all the crystal samples to reach the saturation point of the refractive index change. Two exemplary curves for an undoped sample in the 90°-writing geometry are plotted in figure 4 for different pulse energies and repetition rates. As expected, the dynamics with different parameters for the pulses suggest a dependence of the pulse energy from the steady state refractive index change. It is observable that higher diffraction values could be obtained if the repetition rate was decreased to less than 1 Hz and the energy per pulse amounts to 300 mJ. In figure 4 the saturation diffraction efficiency is plotted against the fluence for undoped and holmium doped crystals. It can be clearly recognized that the saturation value of the diffraction efficiency is dependent on the pump intensity. Refractive index changes are lower than those under continuous illumination and the optimal write intensity is 400 mJ cm^{-2}. Higher values only involve larger absorption changes in the crystal.

4. Data storage

Experiments with the aim of storing large amounts of binary data have to be performed in the 90° configuration (figure 5). The main advantages of the 90° geometry are insensitivity to holographic scattering and fanning as well as a high angular selectivity [47], which is of major importance when aiming for superimposition of many holograms in one storage location. Since Bi_2TeO_5 is biaxial, increased scattering due to birefringence is expected from geometries with no perpendicular incidence. In order to record analog and digital data, a reflective LCOS spatial light modulator with polarization states configured to amplitude only operation is used to imprint the information onto the expanded collimated laser beam. The intensities with a modulated data page and a sparseness of 50% are equal before superposition inside the

crystal. If the signal beam is focused into the storage material and interferes with the reference wave in the Fourier plane a faster recording speed and better error robustness can be achieved.

4.1. Image fidelity

Analog testpatterns are commonly used to determine the image fidelity of the reconstructed holograms. The entire dynamic range of the medium limits the maximum number of gratings one is able to store with a constant SNR. Because holographic storage systems are noise-limited systems an increase in the SNR equals an increase in capacity. The first analog volume hologram was recorded in Bi_2TeO_5 in 2000 [32] and its durability has been investigated in the dark (sequential reading) and during permanent read-out. The SNR of Bi_2TeO_5 samples under pulsed excitation has also been studied [46]. For undoped samples the common SNR under the same storage conditions is 6.0 dB compared with lithium niobate samples with about 11.8 dB. The SNR in relation to the transmitted image changes to 23.7 dB for cw transmission and to 17.4 dB for pulsed illumination. In the case of the reconstructed data the SNR for cw amounts to 19.4 dB and for the reconstructed pulses 11.4 dB has been measured. Figure 6 shows the reconstruction of the same analog page under cw illumination. In some cases shadow images are observable, evoked by internal reflections. However, both images propose a similar fidelity down to number 4 in group 3 of the test charts in the specific optical setup. Bi_2TeO_5 has been with angular- and phase-code multiplexing [7, 46].

The factor with a strong influence on the image quality is the inhomogeneity of the beam profile. Pulse laser beams compared with the cw-laser beam are less fitted for data storage applications. Additionally in Bi_2TeO_5, using pulse energies $>5\,\mathrm{mJ\,cm^{-2}}$ gratings are accompanied by an observable change in the absorption spectrum producing a pale spot in the illuminated area that leads to additional deterioration of the image quality. Up to now, these scattering related values still pose problems when addressing high resolution data pages. Theoretically, the phase-conjugated read out [48] may increase the scattering related performance of Bi_2TeO_5, though it significantly increases the system complexity. Multiplexing large amounts of gratings with low crosstalk and close wavevectors is necessary to achieve a high capacity. To test the applicability of Bi_2TeO_5 in a storage system large stacks of holograms have been recorded. The original information is clearly visible, but the PSNR is at least one magnitude higher compared with the pages stored in lithium niobate. Therefore, the capacity is still not competitive to lithium niobate due to smaller refractive index changes, but outstanding progress has been made in recent years to increase the optical quality of Bi_2TeO_5 [10].

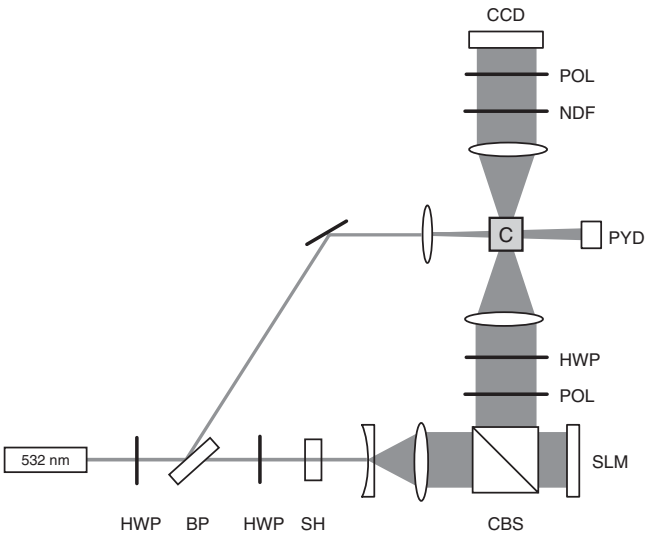

Figure 5. Experimental setup for storage of high capacity data pages with high intensity nanosecond pulses. HWP: half-wave-plate; BR: Brewster plate; SH: shutter; CBS: beamsplitter; POL: polarizer; NDF: neutral-density filter; PYD: pyrodetector; PSM: prism.

4.2. Digital data

The most important figure of merit for digital encoded data pages is the bit-error-rate (BER). When encoding information into binary or multinary brightness levels on an SLM, one defines a classification threshold of the intensity readings on a camera. Bits of information above this classification threshold are decoded as ON bits and below this threshold as OFF bits. The accumulated readings from the detector are commonly plotted depending on their number of occurrences. In these histograms, two peaks appear which represent the ON and OFF bits and are usually placed asymmetrically to

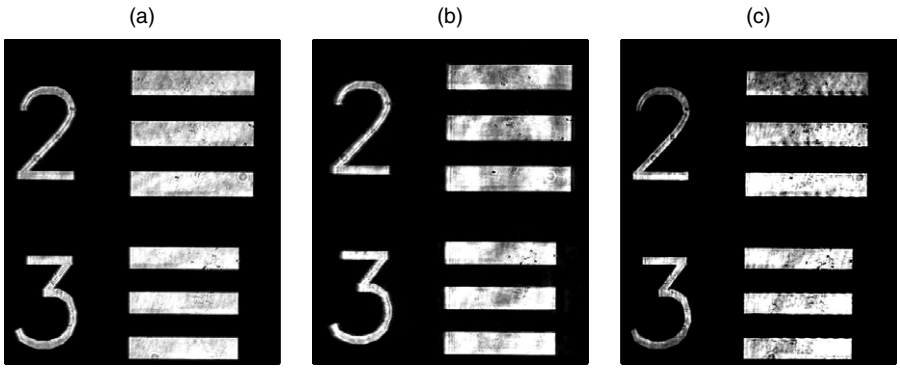

Figure 6. Cut-out of a transmitted USAF testchart. Without crystal (*a*), reconstruction with crystal under cw illumination (*b*) and reconstructed using pulsed illumination (*c*).

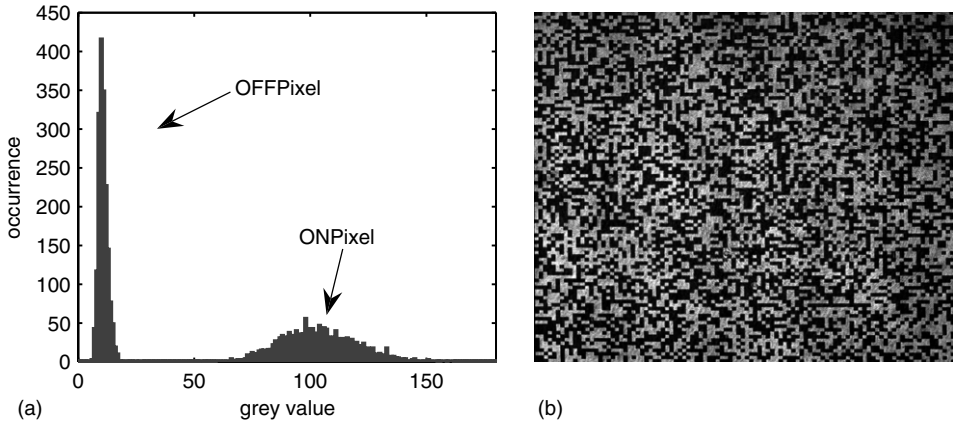

Figure 7. The 8-bit intensity count allocation of logical bits (*a*) and data page with a convenient BER without predistortion (*b*).

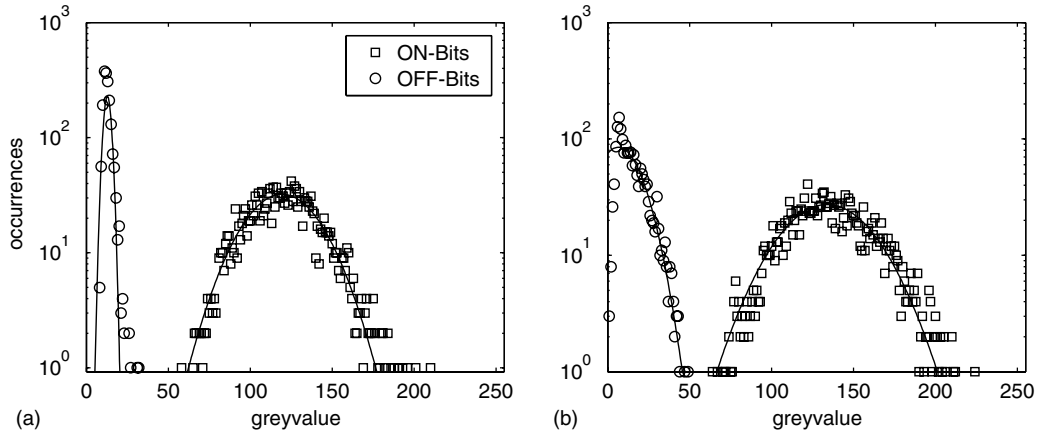

Figure 8. Bit distribution of undoped (*a*) and holmium doped (*b*) crystals for the same set of encoding parameters.

the threshold value. Integrating over the overlapping area of the distribution yields the BER as shown in figure 7 for a data page stored in an undoped Bi_2TeO_5 crystal sample. This method generalizes the error-counting approach. The BER is given by $0.5 \cdot [\int_0^{x_c} W_1(x)\,dx + \int_{x_c}^{\infty} W_0(x)\,dx]$ with the probability distribution W_j and x_c being the crossing point of the distribution [3].

Storing information in the digital bit-pattern also requires considerations about the way data are encoded into physical pixels on an SLM. This is very important for a material such as Bi_2TeO_5, because scattering is always a problem particularly when addressing information with high spatial frequency components. Most common types of data encoding used in the measurements enhance the BER of single or multiplexed data pages and are not directly related to the material properties or the optical system itself, including oversampling, differential encoding [49], modulation coding [50] and adaptive thresholds [51]. Optimized datasets for different Bi_2TeO_5 crystal recursively adapted parameters have already been collected to reduce the BER to a value which is sufficient for binary information storage. In most of the cases it is desirable to achieve a BER of at least 10^{-6}, but the BER itself can be tailored by changing the encoding parameters. In recent experiments a single logical bit was detected using an additional dynamically aligned grid-based algorithm. Persistent landmarks aid the computer supported image compensation to even out deformations and misalignment caused by optical components.

The first page-oriented digital holograms were recorded in Bi_2TeO_5 in 2003, and the BER of the digital holograms was analysed [7, 35]. The starting BER in Bi_2TeO_5 was lower than 10^{-9} and it increased under permanent read-out. However after 7 min it stabilized at about 10^{-4} by the end of the permanent read-out test (45 min). In the reference $LiNbO_3$ crystal the starting BER was much better (10^{-13}) but the hologram faded away during the permanent reading, and the BER became higher than 10^{-2} within 3 min. Figure 8 shows the physical bit distribution decoded from one multiplexed data page in undoped (*a*) and holmium doped (*b*) bismuth tellurite. The parameter set used for encoding the data was the same for both crystals. In particular, an oversampling of 7 has been used which results in a capacity of ca 2.6×10^4 logical bits. The spacing of the binary distribution for undoped bismuth tellurite is much smaller and therefore yields a higher BER than in doped samples.

To compare the BER of bismuth tellurite with competitive materials such as lithium niobate crystals and photosensitive acrylamide polymers [52], several other storage materials have been tested in the system. A sample comparison is shown in figure 9 and includes error rates for a transmitted data page and a page recorded and reconstructed with cw and pulsed illumination, respectively. All of the compared data pages

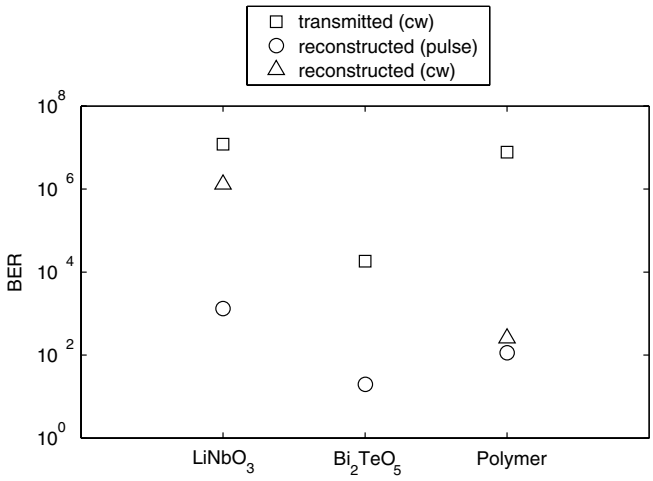

Figure 9. BER comparison of lithium niobate, bismuth tellurite and acrylamide photopolymers used in the same test system with fixed encoding parameters.

have been addressed with the same fixed encoding parameters but different recording schedules adapted to the particular time constants. Although a large variety of dopants has been tested, changing the photorefractive response, the undoped samples still yield the best overall performance in terms of page-wise reconstruction. The storage quality achieved in lithium niobate samples is much higher than in both bismuth tellurite crystals and organic photopolymers.

5. Conclusion

The basic photorefractive parameters of Bi_2TeO_5 and their dependence on the write beam intensity, write beam crossing angle, write beam wavelength and crystal orientation were studied in detail. The durability of holograms without a separate fixing process is a unique property of Bi_2TeO_5 crystals and is the main advantage compared with other photorefractive crystals requiring external electric fields or thermal heating. This behaviour is also observable when using high intensity pulses. The attained diffraction efficiencies are still below those observed in the available thick $LiNbO_3$ samples in the 90° configuration. Additionally Bi_2TeO_5 has been examined in storage systems employing phase-code multiplexing. Digital and analog data pages have been recorded in Bi_2TeO_5 using pulsed signal and reference laser beams. Important parameters for information such as SNR and BER have been determined. Although scattering is still one of the major problems, reconstructed data pages suggested an expedient quality of the material for digital volume holographic data storage in systems. Though it is noticeable that bismuth crystals are still not competitive with lithium niobate in terms of dynamic range and recording speed, major advances have been made concerning growth, dopant concentrations and optical quality to enhance storage dependent parameters.

References

[1] Orlov S S, Phillips W, Bjornson E, Hesselink L, and Okas R 2000 Ultra-high transfer rate high capacity holographic disk digital data storage system *Proc. 29th Applied Imagery Pattern Recognition Workshop (AIPR'00)* p 71, doi:10.1109/AIPRW.2000.953605

[2] Denz C, Pauliat G, Roosen G and Tschudi T 1991 Volume hologram multiplexing using a deterministic phase encoding method *Opt. Commun.* **85** 171

[3] Coufal H J, Psaltis D and Sincebox G T 2000 *Holographic Data Storage* (Heidelberg: Springer)

[4] Breer S, Buse K and Rickermann F 1998 Improved development of thermally fixed holograms in photorefractive $LiNbO_3$ crystals with high-intensity laser pulses *Opt. Lett.* **23** 73

[5] Adibi A, Buse K and Psaltis D 2001 Theoretical analysis of two-step holographic recording with high-intensity pulses *Phys. Rev. A* **63** 023813

[6] Qiao Y, Orlov S, Psaltis D and Neurgaonkar R R 1993 Electrical fixing of photorefractive holograms in SrBaNbO *Opt. Lett.* **18** 1004

[7] Berger G, Denz C, Foldvari I and Peter A 2003 Nonvolatile volume holograms in bismuth tellurite crystals *J. Opt. A: Pure Appl. Opt.* **5** S444–7

[8] Mercurio D, El Farissi M, Frit B and Goursat P 1983 Structural study and sintering of a new piezoelectric material: Bi_2TeO_5 *Mater. Chem. Phys.* **9** 467–76

[9] Gospodinov G and Gyurova K 1985 Synthesis, crystallographic data and thermostability of some metal orthotellurate of the type of Me_3TeO_6 and Me_2TeO_6 *Thermochim. Acta* **83** 243–52

[10] Foldvari I, Peter A, Szakacs O and Munoz A F 1999 Improvement in quality and performance of photorefractive Bi_2TeO_5 *J. Cryst. Growth* **198–199** 482–6

[11] Foldvari I, Peter A, Kappers L A, Gilliam O R and Capelletti R 1992 Basic spectroscopic properties of bismuth tellurium oxide *J. Mater. Sci.* **27** 750–4

[12] Kucha V V, Khomich A V, Kravchenko A B and Perov P I 1984 Growth, structure and optical spectra of bismuth tellurate Bi_2TeO_5 single crystals *Inorg. Mater.* **20** 314–17

[13] Argakov K, Eliseev V, Kudzin A, Sadovskaya L and Sokolyanskii G 1996 Optical absorption in bismuth tellurite *Opt. Spectrosc.* **81** 214–16

[14] Poppl L, Foldvari I and Varhegyi G 2001 Oxidation of bismuth tellurite, Bi_2TeO_5: I. Thermoanalytical and optical microscopic studies *J. Solid State Chem.* **161** 365–72

[15] Klein R S, Fortin W, Foldvari I and Kugel G E 1998 Raman spectra in Bi_2TeO_5 as a function of the temperature and the polarization *J. Phys.: Condens. Mater.* **10** 3659–68

[16] Foldvari I, Peter A, Voszka R and Kappers L A 1990 Growth and properties of Bi_2TeO_5 single crystals *J. Cryst. Growth* **100** 75–7

[17] Peter A, Szakacs O, Foldvari I, Bencs L and Munoz A F 1996 Dopants in photorefractive bismuth tellurite—Bi_2TeO_5 *Mater. Res. Bull.* **31** 1067–73

[18] Avramenko V P, Kudzin A Yu, Reprentcheva S P, Sadovskaya L Ya and Sokolyanskii G H 1988 Electric properties of Bi_2TeO_5 single crystals *Ferroelectrics* **82** 173–8

[19] Kudzin A Yu, Sadovskaya L Ya and Sokolyanskii G Kh 1995 The photocurrent and quantum efficiency in Bi_2TeO_5 single crystals *Ferroelectrics* **174** 85–91

[20] Mandula G, Kovacs L, Peter A and Hartmann E 1992 Refractive index of bismuth tellurium oxide Bi_2TeO_5 *Opt. Mater.* **1** 161–4

[21] Foldvari I, Taheri B, Reeves R J and Powell R C 1993 Nonlinear absorption of laser light in Bi_2TeO_5 single crystals *Opt. Commun.* **102** 245–50

[22] Stabler D L, Amodei J J and Phillips W 1972 Multiple storage of thick holograms in $LiNbO_3$ *Int. Quantum Electronics Conf. VII*

[23] Rakuljic G A, Levya V and Yariv A 1992 Optical data storage by using orthogonal wavelength-multiplexed volume holograms *Opt. Lett.* **17** 1471–3
[24] Barbastathis G, Levene M and Psaltis D 1996 Shift multiplexing with spherical reference waves *Appl. Opt.* **35** 2403–1417
[25] Curtis K, Pua A and Psaltis D 1994 Method for holographic storage using peristrophic multiplexing *Opt. Lett.* **19** 993–4
[26] Denz C, Müller K-O, Heimann T and Tschudi T 1998 Volume holographic storage demonstrator based on phase-coded multiplexing *IEEE J. Sel. Top. Quantum. Electron.* **4** 832
[27] Gunter P and Huignard J-P (ed) 2007 *Photorefractive Materials and their Applications* vol 2 (New York: Springer)
[28] Solymar L, Webb D J and Grunnet-Jepsen A 1996 *The Physics and Applications of Photorefractive Materials* (Oxford: Calderon)
[29] Foldvari I, Scripsick M P, Halliburton L E and Peter A 1991 Photorefractive effect in Bi_2TeO_5 single crystals *Phys. Lett.* A **154** 84–6
[30] Foldvari I, Liu H and Powell R C 1992 Characteristics of the photorefractive effect in Bi_2TeO_5 *Nonlinear Optics III, Proc. SPIE* **1626** 9–20
[31] Foldvari I, Liu H, Powell R C and Peter A 1992 Investigation of the photorefractive effect in Bi_2TeO_5 *J. Appl. Phys.* **71** 5465–73
[32] Foldvari I, Peter A, Denz C, Petter J and Visinka F 2000 Bismuth tellurite—a new material for holographic memory *Opt. Commun.* **177** 105–9
[33] Kogelnik H 1969 Coupled wave theory for thick hologram gratings *Bell. Syst. Tech.* **48** 2909–47
[34] Foldvari I, Denz C, Berger G and Peter A 2002 Holographic performance of photorefractive Bi_2TeO_5 crystals *Radiat. Eff. Defects. Solids.* **157** 1145–8
[35] Berger G, Muller K-O, Denz C, Foldvari I and Peter A 2003 Digital data storage in a phase-encoded holographic memory system: data quality and security *Advanced Optical Storage* ed H J Coufal *Proc. SPIE* **4988** 104–11
[36] Kling A, da Silva M F, Soares J C, Foldvari I and Peter A 2002 Determination of the erbium lattice site in bismuth tellurite using PIXE/channelling *Nucl. Instrum. Methods. Phys. Res.* B **190** 556–9
[37] Foldvari I, Kappers L A, Bartram R H, Capelletti R and Peter A 1998 Photochromic effects in Bi_2TeO_5 : Cr crystals *Opt. Mater.* **10** 47–53
[38] Bencs L, Szakacs O and Kantor T 1999 Determination of erbium and neodymium dopants in bismuth tellurite crystal by graphite furnace atomic spectrometry techniques *Spectrochim. Acta* B **54** 1193–206
[39] Foldvari I, Munoz A F, Camarillo E, Peter A and Szakacs O 1999 Basic spectroscopic properties of Bi_2TeO_5 : Er single crystals *Radiat. Eff. Defects Solids* **149** 55–9
[40] Foldvari I, Munoz A, Camarillo E, Peter A and Sosa R 2000 Basic optical absorption of Er in Bi_2TeO_5 single crystals *Opt. Mater.* **14** 137–44
[41] Dominiak-Dzik G, Ryba-Romanowski W, Lisiecki R and Foldvari I 2007 Spectroscopic properties of Tm^{3+} : Bi_2TeO_5 single crystals *Cryst. Res. Technol.* **42** 1335–40
[42] Dominiak-Dzik G, Ryba-Romanowski W, Foldvari I and Lengyel K 2007 Spectroscopic properties of the Yb^{3+} doped Bi_2TeO_5 single crystal *Opt. Mater.* **30** 139–42
[43] Foldvari I, Baraldi A, Capelletti R, Magnani N, Sosa R, Munoz A, Kappers L A and Watterich A 2007 Optical absorption and luminescence of Ho^{3+} ions in Bi_2TeO_5 single crystals *Opt. Mater.* **29** 688–96
[44] Glass G A M, von der Linde D and Negran T J 1974 The photovoltaic effect and the charge transport in $LiNbO_3$ *Appl. Phys. Lett.* **25** 233–5
[45] Foldvari I, Powell R C, Liu H and Peter A 1993 Four-wave mixing in Bi_2TeO_5 crystal induced by picosecond pulses *Opt. Mater.* **2** 175–84
[46] Horn W, Berger G, Denz C and Foldvari I 2005 Holographic recording in Bi_2TeO_5 using nanosecond pulses *OSA Trends Opt. Photon.* **99** 616–22
[47] Burr G, Mok F and Psaltis D 1995 Angle and space multiplexed holographic storage using the 90° geometry *Opt. Commun.* **117** 49
[48] Burr G and Shelby R 1999 Pixel-matched phase-conjugate readout for holographic data storage *PIE Conf. on Advanced Optical Memories and Interfaces to Computer Systems II* vol 3802 p 24
[49] Heanue J F, Bashaw M C and Hesselink L 1994 Volume holographic storage and retrival of data *Science* **265** 749–52
[50] Burr G W, Ashley J, Coufal H, Gryier R K, Hoffnagel J A, Jefferson C M and Marcus B 1997 Modulation coding for pixel-matched holographic data storage *Opt. Lett* **22** 639–41
[51] Shen X A, Nguyen A D, Perry J W, Huestis D L and Kachru R 1997 Time-domain holographic digital memory *Science* **278** 96–100
[52] Sherif H, Naydenova I, Martin S, McGinn C, Berger G, Denz C and Toal V 2005 Study of an acrylamide-based photopolymer for use as a holographic data storage medium *Proc. SPIE* **5827** 305